

## **Impact of internal waves on sound propagation off Bhimilipatnam, East coast of India**

B.Sridevi, T.V. Ramana Murty, Y. Sadhuram, M.M.M. Rao, K. Maneesha, S. Sujith Kumar and P.L. Prasanna  
National Institute of Oceanography, Regional center, 176, Lawsons bay colony Visakhapatnam-530 017, India

### **Abstract:**

Internal waves (IWs) are identified off Bhimilipatnam, East Coast of India, from the time series CTD (hourly interval) and thermistor chain data (2 minute interval) collected during 23 – 25 Feb, 2007. The measurements were carried out at 94 m water depth on the continental shelf edge. These data sets are used to describe the characteristics of IWs and their impact on acoustic fields. Garrett and Munk (GM) model has been used to predict the characteristics of low frequency (LF) IWs with space and time. Active IWs are seen in the layer 54 m – 94 m with a velocity of  $0.548 \text{ km hr}^{-1}$  and the wavelengths of the order of 0.03 km to 21.8 km. The model could capture the IW features in the thermocline region accurately than at the bottom. This could be due to the limitation of the model which considers linearity. High frequency IWs observed at the bottom could be due to the advection of tidal currents over the shallow irregular bottom in the presence of stratification. The study emphasizes linear IWs rather than transient non-linear waves induced by tidal interaction with topography.

Acoustic simulation results for low frequency IW field reveal that the Intensity loss anomaly of eigenrays was found to be 2.86 dB to 15.59 dB in the water column and maximum (38.48 dB) was observed at the bottom due to the bottom interaction. Our results are well compared with those reported earlier from simulation and acoustic field experiments in the Northern Indian Ocean.

**Key words:** Low frequency, Internal waves, Thermistor chain, GM model, acoustic simulation, East Coast of India

## 1. Introduction:

Oceanic IWs are one of the most ubiquitous features on continental shelves (Fu and Holt, 1982). There are many hypothesized causes, including meteorological conditions (winds and pressure changes), tides and flow over complex bottom topography, surface waves, submarine earthquakes, landslides, and shear flow instabilities. They occur in the regions of strong vertical stratification, such as the thermocline and produce unanticipated variability in measurements (La fond, 1962). Typical vertical scales are around 10 m and the horizontal are from a few hundred meters to kilometers. Temporal scales are of the order of hours, bounded by a minimum inertial frequency (a function of latitude) and a maximum at the Brunt-Vaisala frequency ( $N^2$ ) (Robinson and Ding Lee, 1994).

Physical oceanographers are interested to study the variability of ocean environment rather than it's mean. Oceanic changes relevant to underwater acoustics are classified into mean and fluctuating components (De Santo 1979) with the following general model of the sound velocity equation

$$C(r, t) = C_o(z) + \delta C_1(r) + \delta C_2(r, t) \quad (1)$$

*r - three dimensional position; t - time; z - depth*

having characteristics: 1) a mean vertical profile  $C_o(z)$  that represents local climatology ( $C_o \sim 1500 \text{ m s}^{-1}$ ), 2) a meso-scale component ( $\delta C_1(r)$ ) (fronts, eddies) -- deterministic with respect to the acoustic time scale ( $\delta C_1 / C_o \sim 10^{-2}$ ), and 3) a statistical component ( $\delta C_2(r, t)$ ) (i.e random with respect to the acoustic time scale,  $\delta C_2 / C_o \sim 10^{-4}$ ) that represents small scale fluctuations caused by Internal Waves (IWs) (fine and micro structure). The IW of semi diurnal frequency - internal tides dominates the low frequency (LF) band of IW, while IW of  $> 0.5$  cph dominate the high frequency (HF) band of IW (Murthy, 2002).

IWs are present in all levels of the water column, in deep ocean as well as in marginal coastal areas. As the IWs oscillate underwater, they are potentially dangerous for submarines, off-shore platforms and ships. Ocean engineers' interest in IWs is due to their role in submarine detection and the generation of anomalous drag on ships in fjords and some estuaries. In addition to simulation by numerical modeling, field observation is one of the most important approaches to study the IW. Though ordinary gravity waves are easily seen in day-to-day life, their measurements at Sea are complex. These waves are identified from SAR images (Xiaofeng Li, et al. 1999), shipboard Radar (Dong-Jiing Doong et.al, 2007), special instrumentation like Isothermal follower and thermistor chain etc. (Garrett and Munk, 1979).

Till 1980, around the Indian coast, most of the IW studies (Murthy, 2002) are made utilizing the time series bathythermograph data (La Fond and Rao, 1954, La Fond and La Fond, 1968, Ramam

et.al., 1979) from the stationary ships at fine resolutions for periods up to 3 weeks. After 1980's, the field measurements on IW were mostly made from moored buoys equipped with current meters or with thermistor string (Murthy and Murthy, 1986, ; Shenoj and Antony, 1991; Murthy et.al., 1999, Kumar et.al., 2001) and Satellite sensors (Nath and Rao, 1989; Fernandes et.al., 2000). The time series measurements made from stationary ships and from buoys at different places in the seas around India indicated prominent IW of tidal (0.08 cph) and high (1 – 10 cph) frequencies. The high frequency IWs were found to exhibit diurnal variability with stronger activity during night-time compared to day-time under the influence of local winds. The acoustic intensities can be expected to respond to this diurnal variability. The above studies are confined to thermocline and no information is available at the bottom. The generation of IWs due to the bottom topography and their impact on acoustic propagation characteristics are presented in this study.

In this study predicted sound velocity realizations (with space and time) have been generated by using the statistical universal spectrum GM model. The model incorporates more observational data when compared with any other model and it has been widely accepted by the scientific community (Appendix – A). Acoustic ray model simulation (Ramana Murty et.al., 2005) has been carried out in the presence and absence of model generated IW field which is useful for naval operations.

## **2. Methodology:**

### **2.1 Seafloor Topography off Bhimilipatnam:**

During the winter season (Dec – Feb), the study area experiences northeasterly winds with magnitude of 3.0 to 6.0 m s<sup>-1</sup>. The tides in this region are semi diurnal. The mean spring tidal range is 1.43 m and the neap tidal range is 0.54 m at the nearest port (Visakhapatnam). SST varies from 25 – 26<sup>o</sup> C while at 50 m depth the temperature varies from 26 – 27<sup>o</sup> C which indicates inversion. This is a common feature in this region and the details can be found in an earlier study (Pankajakshan et.al., 2002). Salinity at surface varies from 27 – 32 psu, at 50 m it varies from 32 – 34 psu and about ≈ 35 psu at 100 m depth. The magnitude of currents varies from 20 - 40 cm s<sup>-1</sup> and the direction varies from southwest to northeast from December to February (Varkey et.al., 1996).

Knowledge of Seabed topography in the study area is also a prime requisite to understand the pattern of the IWs in the water column. For this purpose, a representative profile of the high resolution shallow seismic survey carried out earlier by National Institute of Oceanography, Regional Center, Visakhapatnam is selected to study the nature of the seabed topography in the area comprising continental shelf and the upper slope regions off Bhimilipatnam (Fig.1). The figure 1a depicts the location of the observational point and figure 1b shows the cross-sectional seabed topography along AA'. This profile gives general nature of the seabed in terms of sediment quality and morphology. The

seismic record of this region, in general, reveals strong reflectors of the seafloor associated with prominent morphological features such as reefs and pinnacles of varying relief's in the outer shelf regions. A well developed and prominent dome shaped reef feature with significant relief of 10 to 15 m was noticed at the continental shelf edge (around 100 m depth) up to where the gradient of the shelf is found to be moderate and it is abruptly turned to be very sharp and the seabed depth suddenly increases to very higher depths of some hundreds of meters to some thousands of meters. This sharp change in the bathymetry is due to the change in the bottom morphology from the continental shelf to slope. The change in the bottom morphology off Bhimilipatnam from shelf to slope characteristics takes place around the water depth of about 100 m. This part of the shelf is considered as paleo shore line and got submerged due to Holocene transgression (Mohan Rao and Rao, 1994).

## **2.2 Field Program:**

Time series data (2 min interval) on temperature at five depths (5 m, 25 m, 50 m, 75 m and 94 m) have been collected using Thermistor chain during the period 23 – 25 Feb 2007. The sensors have fast response ( $\approx 10$  seconds) and the measuring range is 0 - 45<sup>0</sup>C with an accuracy of  $\pm 0.1^0$  C. Time series CTD data (hourly) had been obtained from SBE 19 plus Seacat profiler (Make: Seabird Electronics, USA).

## **2.3 Modeling of Internal Waves**

The IW parameters vary with space and time. The successful modeling of IW provides the parameters at any interested site in the sea. Garrett and Munk (GM) (1975) succeeded in modeling deep water IW and later it was modified for shallow water IW (Munk, 1981). The model requires time-series temperature data field for frequency analysis and CTD data for Brunt-vaisala frequency, for stratification parameter to provide initial and boundary conditions. For more details on IW modeling one may refer to Krishna Kumar & Balasubramanian (2005) where in the frequency domain was used as one of the inputs. In the present numerical simulation experiment, the wave number domain was used for generation of IW field ( $\delta C_2(r,t)$ ). IW eigen-frequencies and modes at a specified sequence of horizontal wave numbers are computed by using “finite difference – Sturm sequence – bisection – inverse iteration method”, with mean profile. From the model calculations, sequences of sound speed realizations are obtained. Using the temporal and spatial distribution of sound velocity realizations, the range-independent and range-dependent numerical ray tracing experiments are conducted to obtain eigenrays and transmission losses etc., to study the impact of IW on sound propagation.

### 3. Results and Discussion:

#### 3.1 Observations:

##### 3.1.1 Temperature:

Time series data of temperature obtained from the thermistor chain at five depths (5 m, 25 m, 50 m, 75 m and 94 m) are presented in Fig.2. From this figure one can say that small sub surface temperature inversions are observed at 25 m depth. The other interesting feature noticed from this figure is the sharp temperature fluctuations at 50 m and 75 m depths where the layer is highly stratified. These fluctuations are so sharp ---- at times within a span of 40 – 80 minutes, the temperature drops by 2.8<sup>o</sup> C to 0.5<sup>o</sup> C. High oscillations observed at bottom are due to the horizontal shear of the tidal currents over the shallow irregular bottom in the presence of stratification (Leipper, 1955). One of the parameters required for model is the energy factor ( $E_o$ ) which can be estimated from time series data. In order to compute  $E_o$  amplitudes and phases of IWs are needed. For this purpose, the temperature( $T(z,t)$ ) and vertical displacement ( $\eta(z,t)$ ) of pycnocline due to IW expressed in terms of ensemble mean ( $\bar{T}(z)$ ), tidal constituents ( $\omega_i$ ) as follows (Chiswell, 2000).

$$T(z,t) = \bar{T}(z) + \sum_{i=1}^n T_i(z) \cos(\omega_i t - \phi_i^T(z)) \quad \dots\dots\dots (2)$$

$$\eta(z,t) = \sum_{i=1}^n \eta_i(z) \cos(\omega_i t - \phi_i^n(z)) \quad \dots\dots\dots (3)$$

where  $z$  is the depth array,  $t$  is the time array,  $n$  is the number of tidal frequency. The vertical displacements for each tidal constituent can be estimated by dividing the amplitude functions by the vertical gradient i.e.,  $\eta_i(z) = T_i / (\frac{\partial \bar{T}}{\partial z})$ . The functions of  $\phi_i^T(z)$  and  $\phi_i^n(z)$  represent phases corresponding to temperature and displacement. Once amplitudes and phases of displacement function ( $\eta(z,t)$ ) of IWs are computed,  $E_o$  [= Potential Energy (PE) + Kinetic Energy (KE) + Baroclinic potential energy (BPE)] can be estimated from the following equations (Chiswell, 2000).

$$\langle PE \rangle = \frac{1}{2T} \int_0^T \rho g \eta^2(t) dt \quad \text{and} \quad \dots\dots\dots (4)$$

$$\langle KE \rangle = \frac{1}{2T} \int_0^T \rho H (u^2(t) + v^2(t)) dt \quad \dots\dots\dots (5)$$

$$\langle BPE \rangle = \frac{1}{T} \int_0^T \frac{1}{2} \int_{-H}^0 \rho(z) N^2(z) \eta^2(z, t) dz dt \quad \dots\dots\dots (6)$$

where  $\eta, u, v, T, \rho, H, N$  are the displacement profile, zonal and meridional components of currents, observational period, density, water depth and  $N^2$  respectively. Here  $\langle \rangle$  indicates ensemble average. Equations (4-6) have been performed by cubic spline method (Ralston and Wilf, 1967).

Diurnal amplitudes are half of those of the semi diurnal in the water column. Maximum amplitudes of 3.4 m and 7.0 m were observed at 50 m depth (below mixed layer) for diurnal and semi diurnal tides respectively. An increasing trend in the phase from bottom towards surface on diurnal scale suggested that the displacement functions are bottom trapped. Similar results were reported over the Chatham Rise, east of New Zealand by Chiswell (2000).

**3.1.2 Sound Velocity:**

We choose to present sound velocity profiles (rather than temperature and salinity) because of their direct utility in sonar range prediction models. Sound velocity is computed by Chen and Millero (1977) and its distribution is presented in Fig. 3. From surface to 54 m depth, variation of sound velocity is less and from 54 m to bottom strong velocity gradients are observed because of high stratification (Fig. 3b). Mean profiles of temperature, salinity, sound velocity and Brunt Vaisala frequency are shown in Fig.4. Mild inversion is present in the top 50 m layer (Fig. 4a). An increasing trend in salinity from surface to bottom is quite obvious (Fig. 4b). Brunt Vaisala frequency and sound velocity are maximum at 60 m depth. These results suggest the presence of surface duct in the top 50 m layer.

**3.1.3 Spectrum analysis:**

Time series data have been subjected to Fast Fourier Transform (FFT) algorithm (Cooley and Tukey, 1965) to examine the spectral characteristics of the temperature oscillations (Mahadevan et al. 1987) in the study area - off Bhimilipatnam.

The power spectra (Fig.5) of temperature fluctuations at 5 vertical depths (5 m, 25 m, 50 m, 75 m & 94 m) are computed. This is useful to identify the distribution of the vertical isothermal motion of various frequencies. There is a broad range of wave-frequencies and associated energy, where waves of low frequency are associated with high energy while those of high frequency have low energy (Fig.5). The energy associated with the low frequency is a measure of the effect of stratification, while it doesn't seem to have a definite bearing/relation on the high frequency counterpart. However, power

spectra energy at bottom is relatively higher in contrast to that of surface. The IW spectral energy in the thermocline is the highest compared to other depths (above and below). This phenomenon may be due to the high stratification of water column (Fig. 4d). It is interesting to note that IWs off Bhimilipatnam appear to be generated by the bottom forces (Fig.1). This is possible only when a quasi steady current advects in a stratified ocean and as a consequence, bottom topography generates standing IWs known as “lee waves” (Garrett and Munk, 1979). As the tide is a body force altered by the shape of the basin and sea floor configuration (Fig.1), the topographic gradients result in inducing dynamical interaction with the slopes. The role of internal tides on IWs over a continental shelf had been reported earlier (Rippeth and Inall, 2002). In order to know the stability structure of the water column, we have calculated the Richardson Number ( $R_i$ ) from the time series data on currents close to the study area (Ramana Murty et. al., 2007) and found that  $R_i > 0.25$  which indicates turbulent mixing and thereby suppressing of stratification (Turner, 1973). Hence the tide interaction with the shallow bathymetry of Bhimilipatnam may therefore be relatively get enhanced and liable for (more) conversion of the inertial energy (associated with the tide) in the lower spectrum to higher frequencies as the resulting IW of tidal period breaks up into waves of shorter period (while propagating onshore). The dominant frequencies of IWs are found to be 0.025 - 0.49 cph (LF) and 0.5 – 8 cph (HF), though the upper limit of IW band is the  $N^2$  (18 cph) at a depth of 64 m (Table 1).

### 3.1.4 IW characteristics:

IW characteristics are computed from the time series CTD and thermistor chain data. Brunt Vaisala frequency has been computed from the CTD data. The following equation has been adopted for computation of IW wavelength ( $L$ ) (Antony et. al 1985; Murthy and Murthy, 1986). To compute  $L$ , velocity ( $C_{vel}$ ) is needed in prominent IW field. From Fig.3a, it is found that the active IW field prevails between 54 m and 94 m. IW iso – velocity distribution is plotted (Fig. 3b) in the time dependent manner for the mean values of distribution with 2 m sec<sup>-1</sup> equal interval as described by Murthy and Murthy, (1986) to use in the two-layer density model (Defant,1961) .

$$\text{Wave length } L = C_{vel} t_{per} \quad (7)$$

$$C_{vel}^2 = gh \left[ \frac{\rho - \rho'}{\rho} \right] \quad (8)$$

where,  $h$  is the thickness of the top layer of weak density gradient,  $\rho$  is the mean density of bottom layer of strong density gradient,  $\rho'$  is the mean density of top layer of weak density gradient,  $g$  is the acceleration due to gravity and  $t$  is the IW period (from frequency analysis),

The computed values of  $t_{per}$ ,  $h$ ,  $\rho$ ,  $\rho'$ ,  $C_{vel}$ ,  $L$  and wave number ( $k=2\pi/L$ ) are found to be 0.06 hrs - 40 hrs, 21 m, 1023.27 kg m<sup>-3</sup>, 1023.59 kg m<sup>-3</sup>, 0.548 km hr<sup>-1</sup>, 0.03 km - 21.8 km and 33.33 - 0.05 cycles km<sup>-1</sup> for IWs respectively (Figs 2 & 3b) (Table 1). The calculated buoyancy force ( $F_B = -g(\rho - \rho') = -g\Delta\rho$ ) is positive resulting an upward force (Stefanie and Wojcik 2006). In general, the frequency of wave increases with strengthening of  $F_B$ . In the present case it is increasing from the starting to end of the observational period (Fig 3b). One can infer that band of high frequency IWs are more active during night time which is supported by an earlier study (Murthy, 2002).

Another parameter required for the simulation of IW by the model, is wave number ( $k=2\pi/L$ ) domain instead of frequency domain. The range of  $k$  in LF IW field is found to be 0.05 cycles km<sup>-1</sup> to 0.91 cycles km<sup>-1</sup>. In the present paper, the simulation is confined to study the impact of lower frequency IW field on sound propagation. Apart from the above parameters, total energy ( $6E_o$ ) is needed to supplement input to the GM model. The estimated PE, KE, BPE and  $E_o$  with the observed data (Ramna Murty et.al., 2007) were found to be 0.489 J m<sup>-2</sup>, 0.278 J m<sup>-2</sup>, 0.175 J m<sup>-2</sup> and 1.0 J m<sup>-2</sup> respectively. The following section explains a procedure to generate displacements due to IW with the statistics provided by Garrett – Munk power spectrum (Flatte et al. 1979) and also conversion of displacements into sound velocity realizations (Munk and Zachariasen, 1976).

### 3.2 Internal wave simulation:

To run the model, single profiles on temperature, salinity, Brunt-Vaisala frequency and sound velocity (Fig. 4) and an energy level, latitude, range and time scales, energy density factor ( $E_o$ ), stratification scale ( $B$ ) and bandwidth parameter ( $j_*$ ) are required (Fig. 4). Based on the input profiles of  $N^2$  are generated on uniform mesh, with a depth increment  $\Delta z = 2$  m for the computation of IW modes ( $W(z)$ ) (Eq. A1, Appendix A) and eigen-frequencies ( $\gamma_j^2$ ). These modes oscillate only in the water column, where the IW frequency ( $\omega$ ) is smaller than the  $N^2(z)$ . Outside this region the solutions are evanescent (i.e., exponentially decreasing). From our in-situ observations, it is evident that the modes should oscillate between frequencies  $\omega_1 = 0.025$  cph to  $N^2(z) = 18$  cph (i.e., maximum frequency occurred in active IW field at a depth of 64 m), i.e in terms of wave number ( $k$ ) given by 0.05 cycles km<sup>-1</sup> to 33.33 cycles km<sup>-1</sup> (Table 1). The model has its own limitation i.e., the choice of maximum wave number interval ( $k_{min} = 0.01$  to  $k_{max} = 0.5$ ) containing the majority of energy in the IW spectrum (Evans, 1992). The wave number sampling  $\Delta k$  should span the spectrum of the IW field and is used to



approximate ( $\Delta k$ ), an integral over the spectrum (Eq. A4, Appendix - A). Here,  $k_{\max} = 0.5$  cycles  $\text{km}^{-1}$  is used for the power spectrum. Accordingly we have performed the numerical experiment. A wave number sampling increment of  $\Delta k = 0.01$  cycles  $\text{km}^{-1}$  is used with  $M = 46$  samples between  $k_{\min} = 0.05$  cycles  $\text{km}^{-1}$  to  $k_{\max} = 0.5$  cycles  $\text{km}^{-1}$  and the same is followed for negative wave numbers. The modal band width parameter ( $j_*$ ) ( $=1$  for  $J \leq 2$ ;  $2$  for  $J=3$ ;  $3$  for  $J \geq 4$ ) which depends on the number of modes  $J$  is chosen (Jackson and Elliott 2002). The maximum number of modes ( $J$ ) depend on the depth of the water column ( $H$ ). Therefore, we choose  $J$  ( $=2$  for  $0 < H < 25\text{m}$ ;  $3$  for  $25 \leq H \leq 100\text{m}$ ;  $4$  for  $100 \leq H < 250\text{m}$  and  $5$  for  $H \geq 250\text{m}$ ), the maximum number of modes as suggested by Elliott and Jackson (1998). The above mentioned scheme assumes that the first few lower order modes account for 98% of the total energy in the shallow waters (Krishna Kumar & Balasubramanian 2005). Accordingly we have selected  $j_* = 2$  and  $j = 3$  for the present simulation. A total of  $j = 3$  internal wave modes ( $W(z)$ ) and eigen-frequencies ( $\gamma_j^2$ ) are computed at each of the wave numbers ( $M = 46$ ). In the present analysis, modes of positive wave numbers are only considered. The modes will explain the displacement of isopycnals due to IW. Once the internal eigen values ( $\gamma_j^2$ ) and modes ( $W(z)$ ) are found, they can be used to generate realizations of displacements caused by IWs. An energy density factor of  $E_o = 1$  with our observations is used to generate realizations of displacements. Usually  $E_o = 4$  is adopted for deep waters (Flatte', et al. 1979) Apart from the above parameters, stratification scale ( $B$ ) and extrapolated parameter ( $N_o$ ) are also needed for model and can be computed from the formula  $N(z) = N_o e^{-z/B}$ . A fixed value equal to the inertial frequency has been considered for  $N_o$  (Krishna Kumar & Balasubramanian 2005). Using  $N(z)$  from the observed data  $B$  has been computed and value is found to be 0.091 km. Value of  $B$  is 1 km for deep tropical oceans (Munk and Wunsch, 1979). Utilizing all the above parameters, sound velocity profiles ( $C$ ) are obtained by adding the fluctuations ( $\delta C_2$ ) in the following equation (Munk and Zachariasen, 1976) to the background profile ( $C_0$ )

$$\delta C_2(r, z, t) \cong \left( \frac{dc_p}{dz} \right) \text{Re} \zeta(r, z, t) \quad (9)$$

where  $dc_p/dz$  is the potential sound velocity gradient ( $\text{m s}^{-1}$ ) and  $\zeta(r, z, t)$  the IW displacement function (Eq. A4, Appendix A). For acoustic simulation purpose, sound velocity profiles ( $C$ ) are

generated for every 600 sec (10 minutes) between 0 and 21600 sec (6 hours) and for every 1 km interval between 0 and 30 km. The spatial and temporal dependence of the sound velocity in the LF IW field in the contour form is shown in Fig. 6 (Flatte, et al. 1979). The range dependence of the sound velocity profile is the most important consequence of the IWs, on the temporal and spatial scales selected.

Before conducting acoustical numerical experiments, one has to validate the results of the model with observed features with space and time. The model takes the input of mean sound velocity (back ground) profile of time series at fixed position and generates the fluctuations of sound velocity due to IW with space and time. The sound velocity profiles from CTD data coinciding with the trough or crest of IW are compared with those generated from GM model and found that there is a good agreement between the two in the layers; 60 – 80 m (Fig. 7). It is evident that the model could reproduce the temperature oscillations accurately due to the propagation of IWs. Hence it is presumed that the model could generate good results on spatial scale also. It is interesting to note that GM generated IW features can be well noticed in the thermocline than at the bottom. This may be due to the limitation of model frame work which considers linearity. In the present case the bottom generated IW (Figs 2 & 3) comes under the low and high frequency and hence leads to the non-linear phenomena and unable to reproduce the features of IW by the model. Once realizations of displacements in terms of sound velocity are obtained, they can be used to simulate the acoustic propagation.

### **3.3 Acoustic simulation:**

#### **3.3.1 Eigenrays:**

Many acoustic numerical experiments are carried out for different source-receiver configurations for various ranges in IW field. Same configuration has been taken for range independent and dependent acoustic simulation experiments for obtaining intensity loss anomaly. Few typical examples are presented here. The spatial - independence (Without Internal Waves-WIW) and spatial – dependence (IW) of sound velocity profiles in the LF-IW field (Fig. 6) are used as input (left panel of Fig.8 a & b) to trace the rays between source-receiver configuration at 42.22 m depth for 10 km range, to compute eigenrays (middle panel of Fig.8) (Kinsler and Frey 1962; Ramana Murty et.al, 2005) and their corresponding intensity losses (right panel of Fig. 8). No configuration has been found for deeper water to trace the eigenrays. The bottom is considered to be flat and the sediment type is sand. The bottom thickness is taken as 100m. The compression attenuation is  $1800 \text{ m s}^{-1}$ , shear sound velocity is  $650 \text{ m s}^{-1}$ , compression attenuation is 0.39 dB/m/kHz, shear attenuation is 0.3 db/m/kHz and the sediment density is taken as  $2.0 \text{ g cm}^{-3}$  (Krishna Kumar and Murthy, 2002). The columns 5 to 10 of

Table 2 explain the number of upper ( $p^+$ ) and lower ( $p^-$ ) ray turnings, number of top ( $p_t^+$ ) and bottom ( $p_b^-$ ) ray bonks, and overall total number of ray turnings ( $P^+ + P^-$ ) and bonks [ $(p_t^+) + (p_b^-)$ ]. This information can be used as ray identifier. The ray identifier enables us to identify the rays from their arrival patterns, since the rays usually arrive at the receiver end in groups. There are four classes of rays 1)  $R/R$  (purely refracted both above and beneath the axis,  $p_t^+ = p_b^- = 0$ ) 2)  $SR/R$  (surface reflected and refracted,  $p_t^+ \neq 0, p_b^- = 0$ ), 3)  $R/BR$  (refracted and bottom reflected,  $p_t^+ = 0, p_b^- \neq 0$ ) and 4)  $SR/BR$  (surface and bottom reflected,  $p_t^+ \neq 0, p_b^- \neq 0$ ). From Table 2, one can conclude that all the 18 eigenrays come under  $R/R$  category for range-independent while all the 30 eigenrays under  $SR/R$  category for range-dependent nature among the possible 4 classes. From Fig. 8a, one can notice that all the eigenrays are transgressing between the depths of 42 m to 45 m in active IW field under range-independent case and surface to 43 m in range dependent case. Both the cases revealed that (1) rays emerging with positive (negative) source angles reaching receiver with negative (positive) angles having less (more) number of turning depths. (2) Emerging angles of rays with same sign of receiver angle having equal number of turning depths. But under range-dependent case, even though all the rays comes under  $SR/R$  category, one can see that rays with negative (positive) angles reaching receiver with positive (negative) angles having less (equal) number of top bonks. In both the cases, bottom influence is not seen since the sound energy can not penetrate towards higher refractive media and confined within the IW field. Hence, sub-bottom characteristics may not affect the intensity.

Another example for range of 5 km (shown in Table 2), the simulation results revealed that the source-receiver configuration (a) in thermocline (source depth: 55m and receiver depth: 48m) which has 5  $R/R$  eigenrays for range independent and 3  $SR/R$  for range dependent and (b) near bottom (source depth: 92 m and receiver depth: 92 m) which has 4  $R/R$  eigenrays for independent and one bottom bounced  $R/SR$  eigenrays. Here, both the cases (a & b) are in contrast to the configuration of 9 km (i.e., cases 1&2 mentioned above). The results are similar in case 2 of 5 km and case b of 9 km. While the results under cases 1 and a are contradicting which could be due to the asymmetry of the source-receiver configuration.

### 3.3.2 Intensity:

From Table 2, it can be concluded that the travel times of eigenrays cluster may be due to the anticipated ray path degeneracy (Munk and Wunsch, 1979). To avoid ray path degeneracy, in the present simulation experiment, cumulative intensity loss is also computed (Moler and Soloman, 1970) in the presence of IW and without IW considering the phase shift with sub-surface-duct frequency of

1000 Hz (Urlick, 1975; Murthy and Murthy., 1986) instead of individual ray paths. The anomaly (i.e range dependent minus range independent) explains the impact of IW on acoustic propagation characteristics (Table 2) and found to be 2.86 dB for the range of 9 km whereas, 15.59 dB (in the thermocline) and 38.48 dB (bottom) respectively for the range of 5 km. It is interesting to note that less anomaly found for larger range, may be due to transgression of rays in weak IW field compare to short ranges wherein source-receiver configuration kept in deeper depths of high IW activity. (2) Secondly, near bottom source-receiver configuration for short range, anomaly loss of rays is more for the rays which may be due to bottom interaction (double in the present case) compare to others. In the present analysis, comparison has not been possible for 9 km for active IW field, since no configuration was found for eigenrays. Similar results were reported earlier from simulation and through experiments conducted in the North Indian Ocean (Krishna Kumar and Murty, 2002, Prasad Rao et al., 2003).

#### **4. Discussion and Conclusions:**

The present study describes the results from a 44 hours time series of CTD observations (Sampled every hour) and thermistor chain records (sampled every 2 minutes at five discrete water depths). The measurements were carried out in the upper 100 m of the water column at a location near to the continental shelf edge off Bhimilipatnam (India). The observations were used to analyze and describe characteristics and the variability of the internal wave field and it's acoustic properties (sound velocity). In a second step, the observations were used to provide initial and boundary conditions for an adaptation of the Garrett and Munk model to identify and predict characteristics of the low frequency IW field in the space - time domain, and to ultimately determine the relationship between internal wave characteristics and sound propagation through numerical ray tracing experiments.

Based on the analysis of spectrum, harmonic and stability criteria subject to limited time series data, results reveal that the (i) diurnal vertical tidal displacements are about half of those of the semi diurnal tide. Displacement functions appear to be bottom trapped. Similar results were reported by Chiswell (2000) over Chatham Rise, New Zealand. (ii) At bottom, high temperature oscillations are observed and are attributed to the horizontal shear of the tidal currents over the shallow irregular bottom in the presence of stratification. Tide interaction with the shallow bathymetry may therefore be relatively get enhanced and liable for (more) conversion of the inertial energy (associated with the tide) in the lower spectrum to higher frequencies as the resulting IW of tidal period breaks up into waves of shorter period (while propagating onshore).

It is interesting to note that GM generated IW features can be well noticed in the thermocline but not much at the bottom. This may be due to the limitation of GM frame work which considers the linearity. Acoustic simulation results for low frequency IW field reveal that the (i) sound propagation

takes place along  $R/R$ ,  $SR/R$  and  $R/SR$  rays only (ii) Intensity loss anomaly due to IW was found to be 2.86 dB to 15.59 dB in the water column and maximum (38.48 dB) was observed at the bottom due to the bottom interaction. Our results are well compared with those reported earlier from simulation and acoustic field experiments in the Northern Indian Ocean.

## 5. Acknowledgements:

The authors are grateful to Dr.S.R.Shetye, Director, NIO, Goa, Dr.V.S.N.Murty, Scientist-In-Charge NIO (RC), Visakhapatnam for their interest in this study and the Council of Scientific and Industrial Research (CSIR), New Delhi, India for providing facilities. They would like to thank Naval Research Board (NRB), New Delhi for financial support. The first author B.Sridevi is grateful to CSIR, New Delhi, India for the grant of Junior Research Fellowship during the tenure of which a part of this work was carried out. They would like to thank the anonymous reviewers for their valuable suggestions which helped to improve the original manuscript.

## 6. References:

- Antony, M.K., Murty, C.S., Reddy, G.V., Rao, K.H., 1985. Sub-surface temperature oscillations and associated flow in the western Bay of Bengal. *Estuarine, Coastal and Shelf Science* 21, 823-834.
- Chen, C., Millero, F.J., 1977. Speed of sound in sea water at high pressures. *Journal of Acoustic Society of America* 62, 1129-1135.
- Cooley, J.W., Tukey, J.W., 1965. An algorithm for the machine calculation of complex fourier series. *Mathematica of Computation* 19, 297.
- Chiswell, S.M., 2000. Tidal Energetics over the Chatham Rise, New Zealand. *Journal of Physical Oceanography*, 30, 9, 2452 – 2460.
- Desanto, J. A., 1979. *Theoretical Methods in Ocean Acoustics*. edited by Desanto J A, (Springer-Verlag, New York, 1979) 7- 77; see also Dugan J P, *Oceanography in under water Acoustics* Chapter 5.
- Defant, .A., 1961. *Physical Oceanography*, volume 2. Oxford Pergamon Press, 517- 526.
- Dozier, L.B., Tappert, D., 1978. Statistics of normal mode amplitudes in a random Ocean. I. Theory. *Journal of Acoustic Society of America* 63, 353-365.
- Dong-Jiing Doong., Li-Chung Wu., Chia Chuen Kao., 2007. Internal wave propagation observed by Ship board Radar. *Sea Technology* 48, 42- 45.

- Elliott, A.J. and Jackson, J.F.E., 1998. Internal waves and acoustic variability. Proc. of IEEE conference OCEANS'98. 10-14.
- Evans, R.B., 1992. The existence of generalized eigen functions and multiple eigen values in under water acoustics. Journal of Acoustical Society of America 92, 2024-2029.
- Fernandes, A.A., Sarma, Y.V.B., Menon, H.B., Vethamony. P., 2000. Wave directional spectrum from SAR imagery. Journal of Indian Society of Remote Sensing 28, 9-18.
- Flatte, M., Dashen, R., Munk, W. H., Watson, W., Zachariasen, F., 1979. Sound transmission through a fluctuating Ocean. Cambridge University Press, England, pp.56-57.
- Fu, L.L., Holt, B., 1982. Seasat views oceans and sea ice with Synthetic Aperture Radar. Jet Propulsion Laboratory publication 81-120.
- Garrett, C.J.R., Munk, W.H., 1975. Space-time scales of internal waves: A progress report. Journal of Geophysical Research 80, 291-297.
- Garrett, C.J.R., Munk, W.H., 1979. Internal Waves in the Ocean. Annual Reviews in Fluid Mechanics 11, 339-369.
- Gill, A.E., 1982. Atmosphere-Ocean Dynamics. Academic press, San Diego, USA.
- Jackson, J.F.E. and Elliott, A.J., 2002. Internal waves in the Clyde Sea, Estuarine Coastal and Shelf Science 54, 51-64.
- Kinsler L.E. and Frey A.R., 1962. Fundamentals of Acoustics, John Wiley & Sons, Inc., New York, London pp 522.
- Krishna Kumar, G.V., and Murthy, P.G.: 2002, Simulation of Sound Speed Structure due to Internal Waves in the Ocean. In: *Proc. ICONS – International Conference on Sonar-Sensors and Systems*.
- Krishna Kumar, G.V., Balasubramanian, P., 2005. IWAVE: An Ocean simulation model for internal waves. Current Science 89, 1927-1932.
- Kumar, O.V., Nair, P.V., Kumar, P.V.H., Kumar N.M., Salam, K.A.A., Chandran K.P.B., Venkatachalam, N.R., 2001. Report on the acoustical Oceanography experiment in the shallow waters off Saurashtra coast during Oct-Nov 2000, Technical Report No. RR- 29/2001.
- La Fond, K.G., Rao, C.P., 1954. Vertical oscillations of tidal periods in the temperature structure of the sea. Andhra University Memoirs 1, 109-116.
- Lafond, E.C., 1962. Internal waves. The Sea 1, edited by M.N. Hill, 731- 751, New York, Wiley.
- La Fond, E.C., La Fond, K.G., 1968. Studies on oceanic circulation in the Bay of Bengal. Bulletin of National Institute of Science, India 38, 169 -183.

- Leipper, D.F., 1955, Sea temperature variations associated with tidal currents in stratified shallow water over an irregular bottom. *Journal of Marine Research*, 14(3), 234 -252.
- Mahadevan, R., Swaminathan, T., Issac Martin, M., 1987. Ocean surface wave analysis. Technical Report 27, Ocean Engineering center Indian Institute of Technology, Chennai, pp 115.
- Mohana Rao, K., Rao, T.C.S., 1994. Holocene Sea Level of Visakhapatnam Shelf, East Coast of India. *Journal of Geological Society of India* 44, 685-689.
- Moler, C.B., Solomon, L.P., 1970. Use of splines and numerical integration in geometrical Acoustics. *Journal of Acoustic Society of America* 48, p 739.
- Munk, W.H., Zachariasen, F., 1976. Sound propagation through a fluctuating Ocean: Theory and observations. *Journal of Acoustic Society of America* 59, 818-838.
- Munk, W.H., Wunsch, C., 1979. Ocean Acoustic Tomography: A scheme for large scale ocean monitoring. *Deep - Sea Research* 26, 123-161.
- Munk, W., 1981. In *Evolution of Physical Oceanography*. MIT press, Massachusetts, USA.
- Murthy, P.G.K., Murthy, G.R.K., 1986. A case study on the influence of internal waves on sound propagation in the sea. *Journal of Sound and Vibration* 108 (3), 447.
- Murthy, P.G.K., Viswambharan, N.K., Rao, A.R., Radhakrishnan, V.G., 1999, A note on the Structure of Internal waves in the Coastal waters off Cochin, Reference No. 13/99.
- Murthy, P.G.K., 2002. An Insight Into Internal Waves In the Seas – around India. International Conference on Sonar – Sensors and Systems, Proceedings of ICONS, Kochi, Naval Physical and Oceanographic Laboratory, India.
- Nath, A.N., and Rao, M.V., 1989. Detection of Oceanic waves through multi spectral scanners, Third Nat. Conference on Dock and Harbour Eng. Surathkal, 5-12.
- Pankajakshan, T., Gopala Krishna, V.V., Muraleedharan, P.M., Reddy, G.V., Araligidat, N., Shenoy, S., 2002, Surface layer temperature inversions in the Bay of Bengal, *Deep Sea Research*, Part – I, 49, (10), 1801 – 1818.
- Prasad Rao, C.V.K., Swain, J., Hareesh kumar, P.V., Nair, P.V., Panchalai, V.N., Shukla, R.K., 2003. Underwater acoustic propagation experiments during ARMEX, ARMEX-workshop on Data Analysis and Initial Scientific Results, 22-23 Dec 2003.
- Press, W.H., Teukolsky, S.A., Vetterling, W.T., Flannery, B.P., 1992. *Numerical Recipes in Fortran* Second Edition, 463-475, Cambridge University Press, New York.
- Ralston, A. and Wilf, H.S.:1967, *Mathematical methods for digital computers*, Spline functions, Interpolation and numerical quadrature, *T.N.E. Greville*, pp 156-168.

Ramam, K.V.S., Murthy, P.G.K., Kurup, C.K.B., 1979. Thermal structure variation in the Arabian Sea (May-July 1973). *Mausam* 30, 105-112.

Ramana Murty, T.V., Prasanna Kumar, S., Somayajulu, Y.K., Sastry, J.S., Rui, J.P., De Figueiredo, 1989. Canonical sound speed profile for the central Bay of Bengal. *Journal of Earth System Science*, 255-263.

Ramana Murty, T.V., , Malleswara Rao, M.M., Surya Prakash, , Chandramouli, P., and Murty, K.S.R. 2005, Algorithms and interface for Ocean acoustic ray tracing, Technical Report No. NIO/TR-09/2005, National Institute of Oceanography, Regional Center, Visakhapatnam, India.

Ramana Murty, T.V., Sadhuram, Y., Malleswara Rao, M.M., Sujith Kumar, S., Maneesha, K., Sai Sandhya, K., Surya Prakash, S., Chandramouli, P., Murty, K.S.R., 2007. Identification and Modeling of Internal Waves, Technical Report No. NIO/TR-02/2007, National Institute of Oceanography, Regional Center, Visakhapatnam, India.

Rippeth, T.P., Inall, M.E., 2002. Observations of the internal tide and associated mixing across the Malin Shelf. *Journal of Geophysical Research* 107 (C4), 3028, DOI: 10.1029/2000JC000761.

Robinson, A.R., Ding Lee., 1994. *Oceanography and Acoustics*. AIP Press, pp 257.

Saunders, K.D., 1990. Private communication. Naval Research Laboratory, Stennis Space Center, MD.

Shenoi, S.S.C., Antony, M.K., 1991. Current measurements over the Western continental shelf of India. *Journal of Continental Shelf Research* 11, 81-93.

Stefanie, E, Wojcik, 2006. Effects of Internal waves and Turbulent Fluctuations on underwater Acoustic Propagation, Master of Science thesis, Worcester Polytechnic Institute.

Turner, J.S., 1973. *Buoyancy Effects in Fluids*, Cambridge University Press.

Urick, R.J., 1975. *Principles of under water sound*. 2<sup>nd</sup> ed., McGraw-Hill Book Company, New York. pp. 384.

Varkey, M.J., Murty, V.S.N., and Suryanarayana, A., 1996. Physical Oceanography of the Bay of Bengal and Andaman Sea, eds, A.D. Ansell, R.N. Gibson and M. Barnes, *Oceanography and Marine Biology, An Annual Review*, Vol. 34, UCL Press, 1- 70.

Xiaofeng, Li., John Morrison., Leonard Pietrafesa., Andy Ochadlick., 1999. Analysis of Oceanic Internal Waves from Airborne SAR Images. *Journal of Coastal Research* 15, 884-891.



## Appendix A

### Internal Wave Eigen value and Modes:

Saunders (1990) had developed IW model with guiding principle that maximum simplicity should prevail while producing results that are representative of the IW field based on the following assumptions: (1) linearity, (2) no mean shear, (3) a Boussinesq fluid, (4) flat or slowly varying bottom, and (5) horizontally homogeneous or slowly varying density field. The exact dispersion relation, for the IWs in the density stratified rotated ocean, is the solution of the eigen values as given by Gill (1982).

The internal wave eigen values and modes are determined by water depth  $H$  in meters, the buoyancy frequency profile  $N^2(z)$  and inertial frequency  $\omega_i$  in rad/s. Here  $N(z) = \left[ -\frac{g}{\bar{\rho}} \frac{d\rho}{dz} \right]^{1/2}$ , where  $g$  is the gravitational acceleration, and  $\bar{\rho}$  the mean density of the medium. IW frequencies  $\omega$  are limited to the range between inertial frequency ( $\omega_i$ ) at the lower end and maximum buoyancy frequency ( $N^2$ ) at the higher end. The internal wave modes  $W_i(z)$  satisfy the eigen value problem

$$\frac{d^2 W_j(z)}{dz^2} + \{ \gamma_j^2 [N^2(z) - \omega_i^2] - k^2 \} W_j(z) = 0 \quad 0 \leq z \leq H \quad (A1)$$

where  $W_j(0) = W_j(H) = 0$  and  $k$  is a known spatial wave number in  $\text{rad m}^{-1}$ . The quantities  $\gamma_j^2, j=1, J$  are the eigen values that are related to the eigen-frequencies by the equation  $\omega_j^2 = \omega_i^2 + k^2 / \gamma_j^2$  (Dozier and Tappert, 1978).

The eigen values of Eq. A1, are bounded below by  $k^2_{\max} [N^2(z) - \omega_i^2]$ , as can be established using an extension of the argument given by Evans (1992). Each wave number  $k$  has its own set of infinity depth-dependent vertical modes  $W(z)$  of the system. These modes oscillate only in the region of the water column, where IW frequency  $\omega$  is smaller than the buoyancy frequency ( $N^2(z)$ ). Outside this region the solutions are evanescent. Therefore, the vertical displacement of the linear IW field can be expressed as a combination of plane waves as weighted double sum over mode number

## Displacements:

The complex internal wave displacements, with real and imaginary parts in meters, are taken to have the form [ Dozier and Tappert, 1978].

$$\zeta(r, z, t) = \sum_{j=1}^J \int_{-\infty}^{\infty} A_j(k) W_j(k^2, z) \exp[ikr + i\omega_j(k^2)t] dk \quad (A2)$$

where the  $k^2$  dependence of the internal wave modes and eigen-frequencies are indicated explicitly. The expansion coefficients  $A_j(k)$  are identically distributed complex Gaussian random variables with zero mean. Their variance is given by the Garrett-Munk power spectrum defined by Flatte', et. al. (1979) as

$$P_j(k^2) = E_0 \frac{4}{\pi^2} \frac{3}{j^2 + j_*^2} \frac{k_j k^2}{(k^2 + k_j^2)^2} \quad (A3)$$

where  $k_j = (\pi F_I / BN_0)j$ ,  $B$  the stratification scale, (Ramana Murty et.al., 1989),  $N_0$  extropolated Brunt-vaisala frequency and  $E_0$  the energy density factor. The quantity  $F_I$  is the inertial frequency computed using  $F_I = (1/12) \sin(\text{latitude})$  with units of cycles hour<sup>-1</sup>. Here the number of wave numbers is doubled to account for both positive and negative wave numbers.

Computation of internal wave displacements requires a numerical approximation of integral in Eq. (A2). This starts with a choice of a maximum wave number  $k_{\max}$  to bound the interval that contains the majority of the energy in the internal wave spectrum. For the Garrett-Munk power spectrum this is around 0.5 cycles km<sup>-1</sup> converted into rad m<sup>-1</sup>. The interval  $[0, k_{\max}]$  is divided into  $M$  parts of size  $\Delta k = k_{\max} / M$ . The discrete horizontal wave numbers, used in the internal wave eigen-frequency calculations, are taken to be  $k_m = m\Delta k$ ,  $m = 1, M$ . The integral in Eq. (A2) is approximated, using both positive and negative values of  $m$ , by

$$\zeta(r, z, t) \cong \sum_{j=1}^J \sum_{m=\pm 1}^{\pm M} \sqrt{\frac{P_j(k_m^2)}{\Delta k}} G_{j,m} W_j(k_m^2, z) \exp[ik_m r + i\omega_j(k_m^2)t] \Delta k \quad (A4)$$

where both the real and imaginary parts of  $G_{j,m}$  are Gaussian random variables with zero mean and unit variance and  $r$  is the range,  $z$  is the depth and  $t$  is the time. Independent realizations of  $G_{j,m}$  are generated by calling the subroutine "GASDEV" (Press. et.al., 1992) separately for the real and imaginary parts and for each  $j$  and  $m$  (both positive and negative). Number of random realizations of sound velocity created for the sequence of time and range according to requested number. If an odd number is requested an extra realization is created to make the number of realizations even.

**Sound speed Fluctuations:**

The displacement fields obtained from Eq. (A2) are converted into sound speed fluctuations using the relation from Munk and Zachariasen (1976)

$$\delta c_2(r, z, t) \cong (dc_p / dz) \operatorname{Re} [\zeta(r, z, t)] \quad (A5)$$

where,  $dc_p / dz$  is the potential sound speed gradient in ( $s^{-1}$ ). Here the potential sound speed gradient is used to compute the sound speed realizations caused by the IWs.

## List of Tables and Figures:-

### Tables:

Table 1: Derived characteristics of various components in the IW field

Table 2: a) Acoustic ray parameters (Range-independent)

b) Acoustic ray parameters (Range-dependent)

(source depth = 42 m, receiver depth = 42 m, Range = 10 km)

### Figure Captions

Figure 1: a). Study area

b). Cross-sectional seabed topography along AA<sup>1</sup> (shown in figure 1a)

Figure 2: Time series data of temperature (2 min interval) collected from thermister chain at 5 depths (5 m, 25 m, 50 m, 75 m and 94 m) off Bhimilipatnam during 23 – 25 Feb 2007

Figure 3: a). Variation of sound velocity ( $\text{m}\cdot\text{s}^{-1}$ ) off Bhimilipatnam

b). Sound velocity structure revealing internal waves. A, indicates sound velocity structure after eliminating internal waves. Contour interval is  $2 \text{ m s}^{-1}$ .

Figure 4: Mean profiles of a) Temperature ( $^{\circ}\text{C}$ ) b) Salinity (psu) c) Sound Velocity ( $\text{ms}^{-1}$ ) and d) Brunt-Vaisala's frequency (cph) off Bhimilipatnam during 23<sup>rd</sup> -25<sup>th</sup> Feb 2007

Figure 5: Energy spectra of temperature oscillations at (a) 5 m, (b) 25 m, (c) 50 m, (d) 75 m and (e) 94 m depths off Bhimilipatnam during 23-25 Feb2007

Figure 6: Spatial (a) and temporal (b) dependence of sound velocity distribution in the internal wave field off Bhimilipatnam

Figure 7: Comparison of Sound Velocity profiles between the observed and Model (GM) off Bhimilipatnam (— observed; - - - model)

Figure 8: Ray paths for a) Range-independent b) Range-dependent off Bhimilipatnam

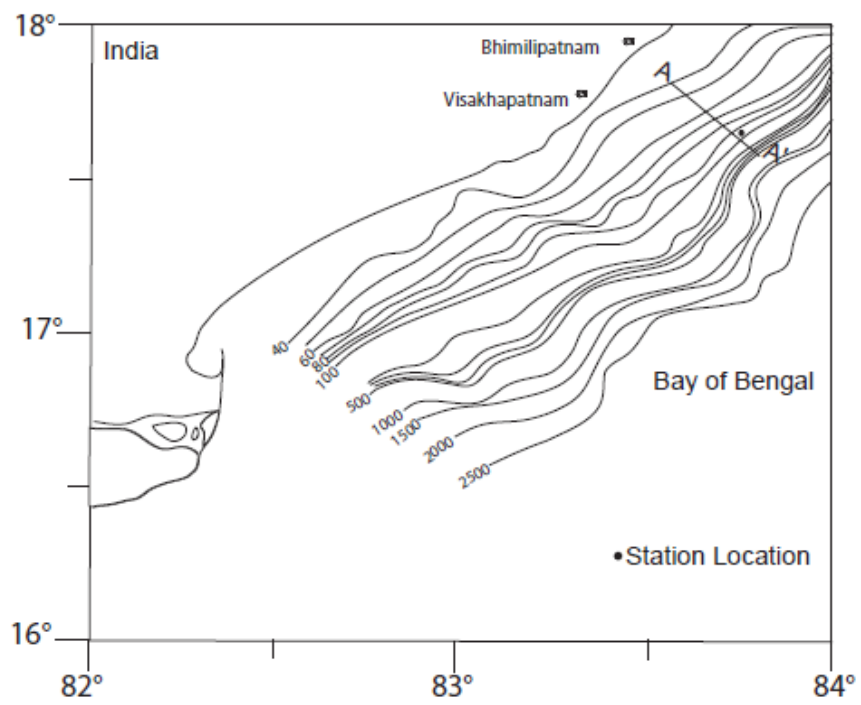


Figure 1a

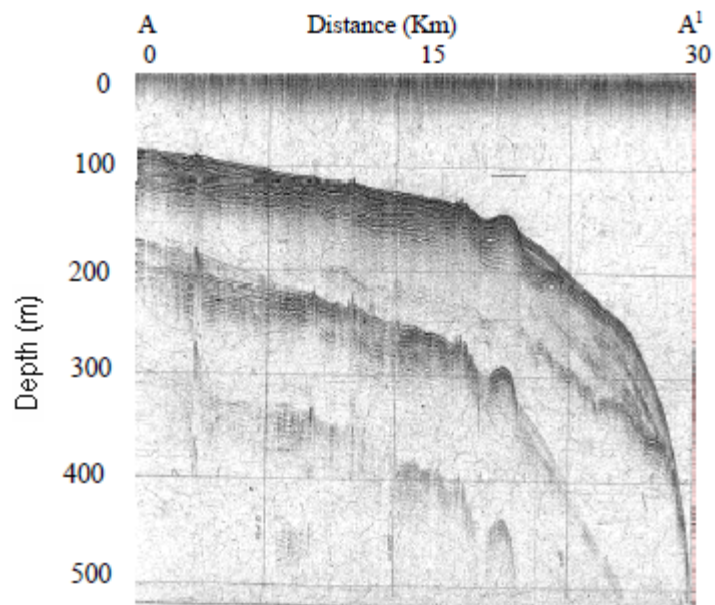


Figure 1b

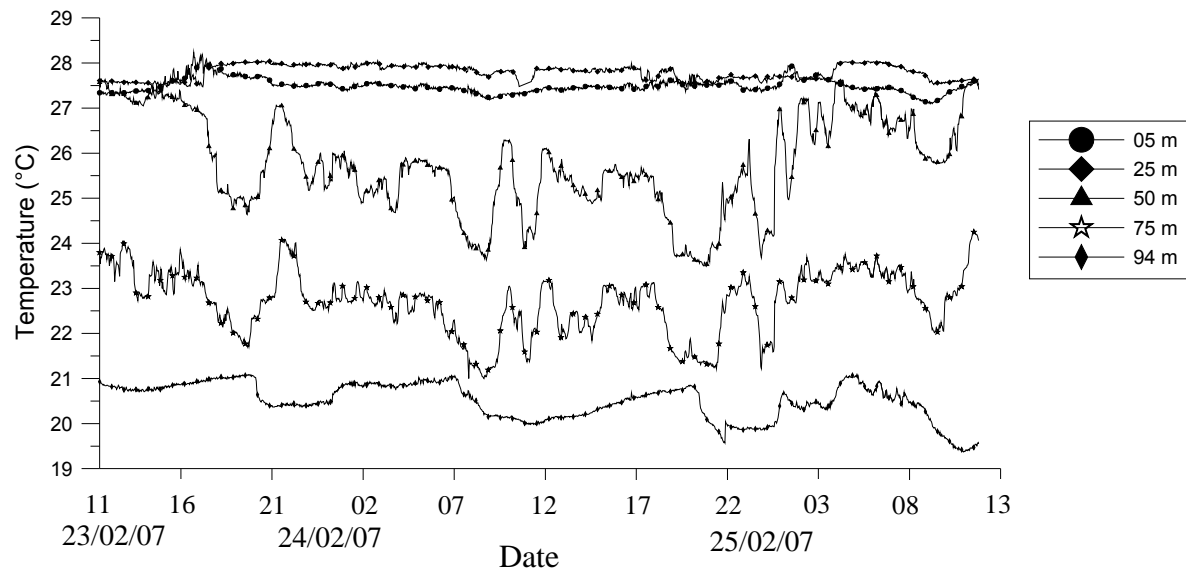


Figure 2

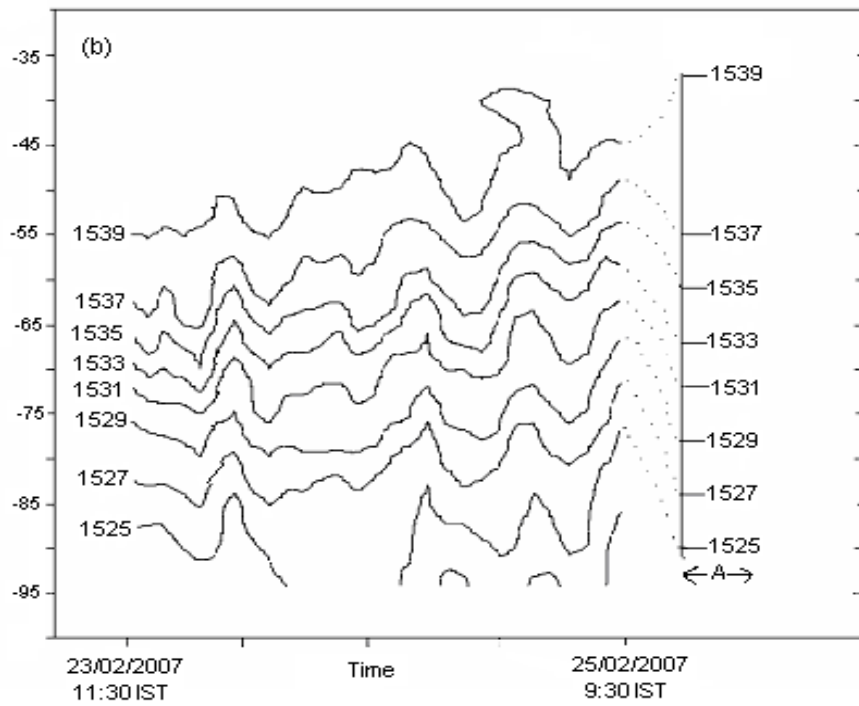
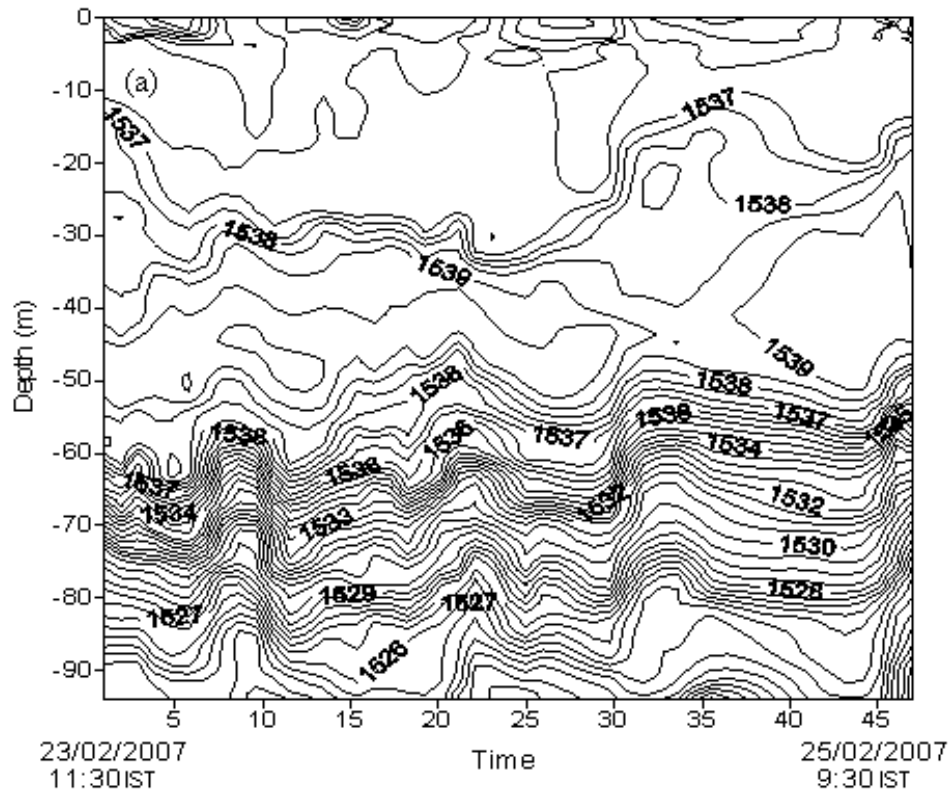


Figure 3

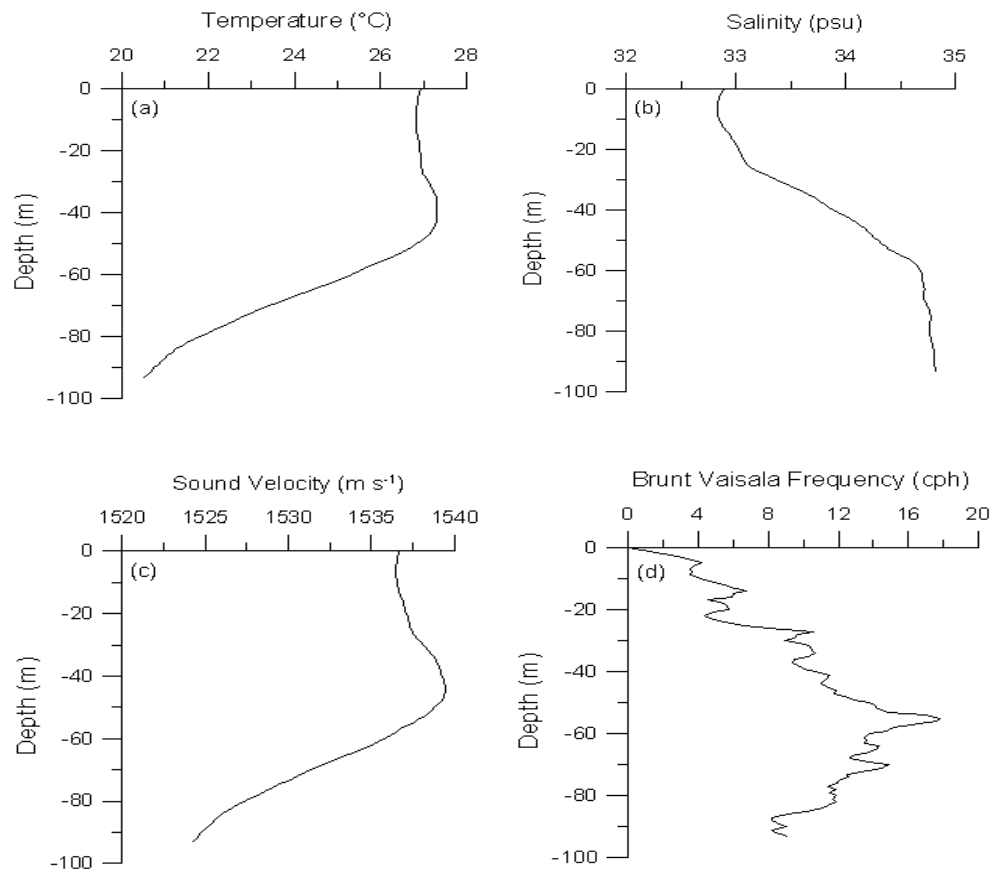


Figure 4



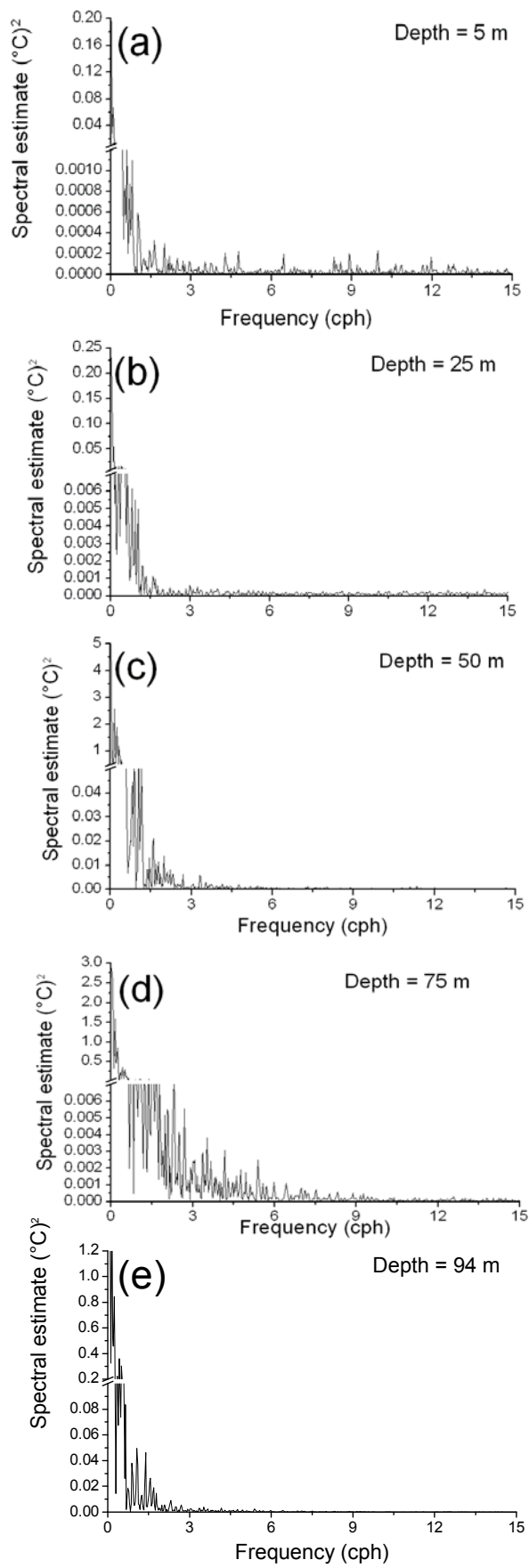


Figure 5

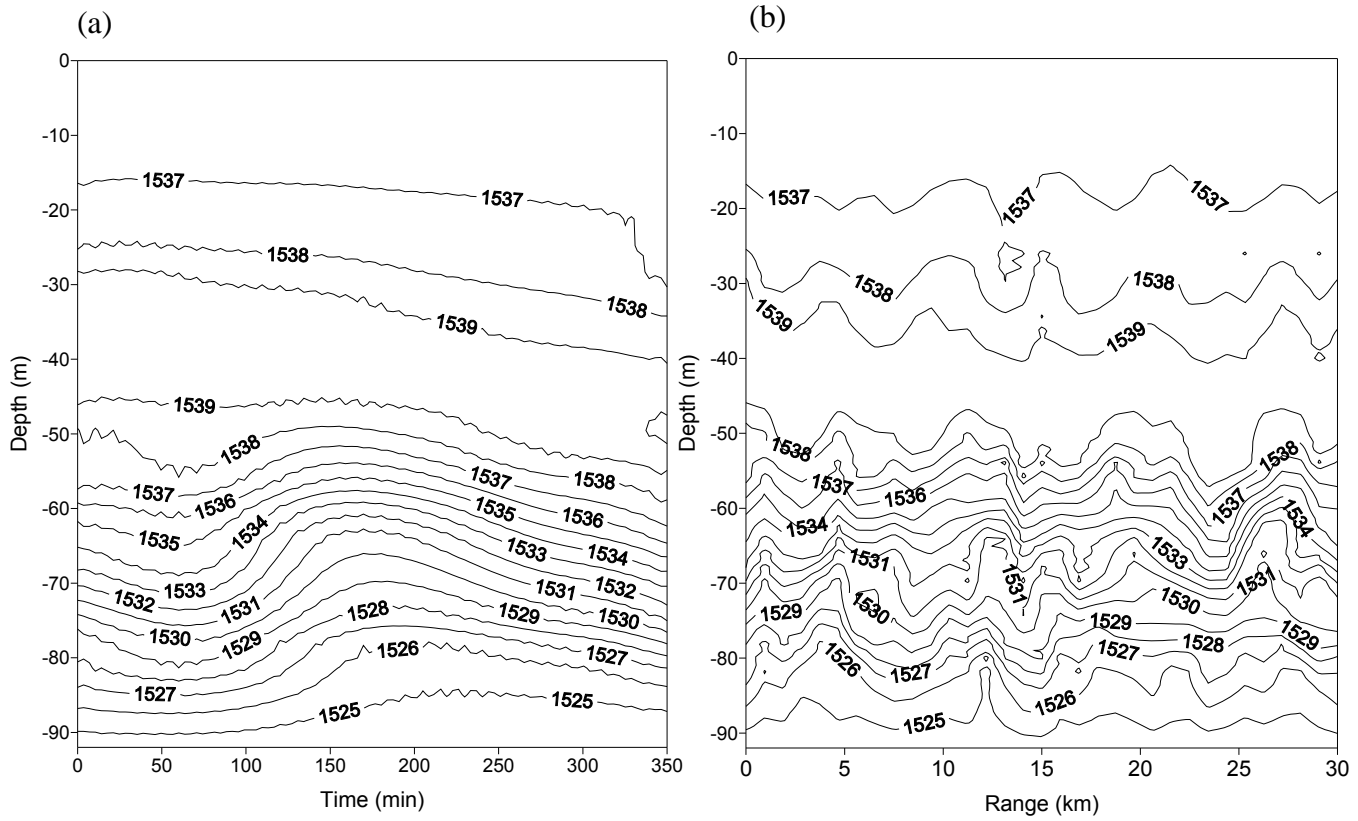


Figure 6

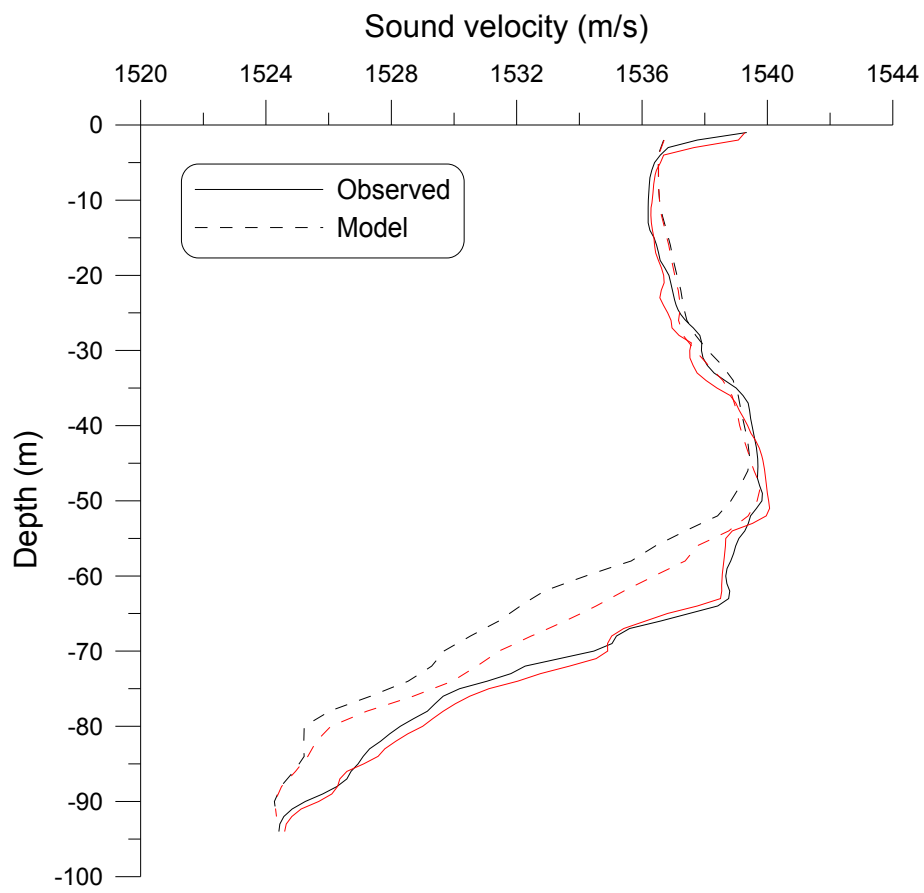
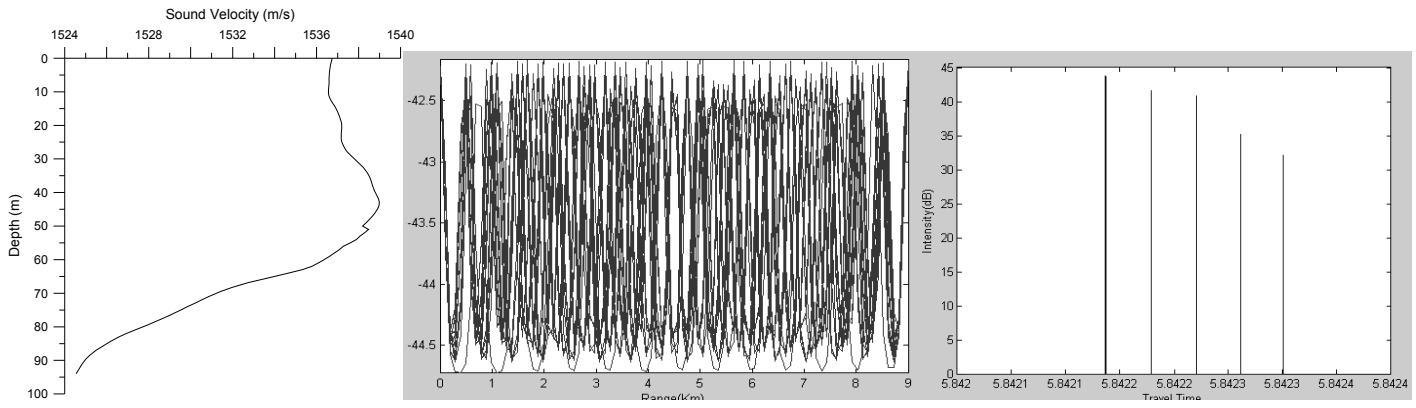


Figure 7

### a) Range Independent



### b) Range Dependent

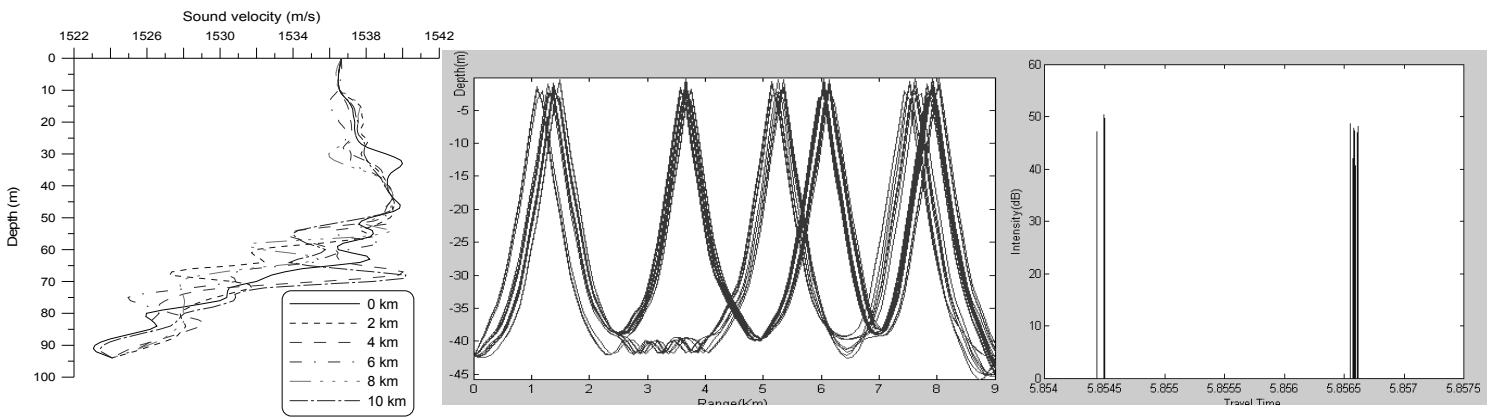


Figure 8

Table 1

S.No	Name of the component	Frequency ( $\omega$ ) (cph)	Time period ( $T$ ) (hrs)	Wave length ( $L$ ) (km)	Wave number ( $k$ ) (cycles/km)
1	Inertial frequency ( $\omega_i$ )	0.025	39.8	21.8	0.05
2	Principal lunar component ( $M_2$ )	0.081	12.7	6.81	0.15
3	Principal solar component ( $S_2$ )	0.083	12	6.58	0.15
4	Upper bound of low frequency IW	0.5	2	1.1	0.91
5	Brunt vaisala frequency ( $N^2$ )	18	0.06	0.03	33.33

Table 2

S.No	$\vartheta_0$ (deg)	$\vartheta_r$ (deg)	$T$ (sec)	$\rho^+$	$\rho^-$	$\rho_t^+$	$\rho_t^-$	$\rho^+ + \rho^-$	$\rho_t^+ + \rho_t^-$	$\Sigma ds$ (m)	$I/I_0$
<b>Range independent:-</b>											
<b>Range : 9 km      Source depth : 42.22 m      Receiver depth : 42.22 m</b>											
1	-0.00327	0.006614	5.8545	5	6	3	0	11	3	9005.7	9.18E-06
2	-0.00323	0.004693	5.8545	5	6	3	0	11	3	9005.6	8.54E-05
3	-0.00208	0.004384	5.8545	5	6	3	0	11	3	9005.5	0.000177
4	-0.0018	0.004794	5.8545	5	6	3	0	11	3	9005.7	1.16E-05
5	-0.00128	0.009991	5.8545	5	6	3	0	11	3	9005.8	8.07E-05
6	-0.00005	-0.0155	5.8566	4	4	4	0	8	4	9007.5	6.08E-05
7	0.004071	-0.0131	5.8566	4	3	4	0	7	4	9007.5	8.79E-05
8	0.004141	-0.01824	5.8566	4	3	4	0	7	4	9007.5	1.81E-05
9	0.004176	-0.0225	5.8565	4	3	4	0	7	4	9007.5	1.75E-05
10	0.004245	-0.01815	5.8566	4	3	4	0	7	4	9007.5	4.91E-05
11	0.00428	-0.02262	5.8565	4	3	4	0	7	4	9007.5	1.37E-05
12	0.00428	-0.02262	5.8565	4	3	4	0	7	4	9007.5	1.37E-05
13	0.004455	-0.01693	5.8566	4	3	4	0	7	4	9007.5	1.91E-05
14	0.004595	-0.01808	5.8566	4	3	4	0	7	4	9007.5	1.65E-05
15	0.004595	-0.01808	5.8566	4	3	4	0	7	4	9007.5	1.65E-05
16	0.0047	-0.01659	5.8566	4	3	4	0	7	4	9007.6	3.22E-05
17	0.004735	-0.01761	5.8566	4	3	4	0	7	4	9007.5	3.96E-05
18	0.004874	-0.01364	5.8566	4	3	4	0	7	4	9007.5	0.000198
19	0.004909	-0.01401	5.8566	4	3	4	0	7	4	9007.5	0.000111
20	0.005014	-0.01749	5.8566	4	3	4	0	7	4	9007.4	6.45E-05
21	0.005084	-0.01666	5.8566	4	3	4	0	7	4	9007.4	4.43E-05
22	0.006237	0.012179	5.8545	5	5	3	0	10	3	9005.8	1.07E-05
23	0.006342	-0.02252	5.8544	5	4	3	0	9	3	9005.6	1.95E-05
24	0.006342	-0.02252	5.8544	5	4	3	0	9	3	9005.6	1.95E-05
25	0.015811	-0.01626	5.8566	4	3	4	0	7	4	9007.6	4.00E-05
26	0.015916	-0.01933	5.8566	4	3	4	0	7	4	9007.5	5.64E-05
27	0.015916	-0.01933	5.8566	4	3	4	0	7	4	9007.5	5.64E-05
28	0.016091	-0.01702	5.8566	4	3	4	0	7	4	9007.7	1.51E-05
29	0.016195	-0.01636	5.8566	4	3	4	0	7	4	9007.7	1.58E-05
30	0.01623	-0.01888	5.8566	4	3	4	0	7	4	9007.7	1.96E-05
<b>Range dependent:-</b>											
<b>Range : 9 km      Source depth : 42.22 m      Receiver depth : 42.22 m</b>											
1	-0.00554	0.002086	5.8422	15	16	0	0	31	0	9000.5	4.25E-05
2	-0.0055	0.001092	5.8422	15	16	0	0	31	0	9000.5	5.32E-05
3	-0.0047	0.003522	5.8423	17	18	0	0	35	0	9000.5	0.000213
4	-0.00466	-0.00478	5.8423	18	18	0	0	36	0	9000.5	0.000157
5	-0.00383	0.003929	5.8423	18	19	0	0	37	0	9000.5	0.000566
6	-0.00379	-0.00111	5.8423	19	19	0	0	38	0	9000.5	0.000304
7	0.001869	-0.00129	5.8424	21	20	0	0	41	0	9000.5	0.000613
8	0.001904	0.002301	5.8424	20	20	0	0	40	0	9000.5	0.000763
9	0.003721	-0.00393	5.8423	20	19	0	0	39	0	9000.5	0.000377
10	0.003756	0.001465	5.8423	19	19	0	0	38	0	9000.5	0.000404
11	0.004595	-0.00434	5.8423	19	18	0	0	37	0	9000.5	8.28E-05
12	0.004595	-0.00434	5.8423	19	18	0	0	37	0	9000.5	8.28E-05

13	0.004665	0.004638	5.8423	18	18	0	0	36	0	9000.5	0.000374
14	0.004665	0.004638	5.8423	18	18	0	0	36	0	9000.5	0.000374
15	0.005154	-0.00541	5.8422	18	17	0	0	35	0	9000.5	6.92E-05
16	0.005224	0.002683	5.8422	17	17	0	0	34	0	9000.5	7.16E-05
17	0.005503	-0.00098	5.8422	17	16	0	0	33	0	9000.5	4.13E-05
18	0.005503	-0.00098	5.8422	17	16	0	0	33	0	9000.5	4.13E-05
<b>Range independent:-</b>											
<b>Range : 5 km    Source depth : 48 m    Receiver depth : 55 m</b>											
1	-0.02014	-0.007	3.2475	4	4	0	0	8	0	5000.7	6.49E-09
2	-0.01758	-0.00758	3.2475	4	4	0	0	8	0	5000.6	6.18E-08
3	-0.01712	0.011208	3.2475	3	4	0	0	7	0	5000.5	2.40E-08
4	0.016883	0.007553	3.2475	3	3	0	0	6	0	5000.5	1.64E-08
5	0.017116	-0.01142	3.2475	4	3	0	0	7	0	5000.5	3.51E-08
<b>Range dependent:-</b>											
<b>Range : 5 km    Source depth : 48 m    Receiver depth : 55 m</b>											
1	0.052075	-0.01584	3.2509	3	2	1	0	5	1	5002.3	2.30E-10
2	0.053614	-0.06016	3.2511	4	3	1	0	7	1	5002.5	9.04E-11
3	0.05484	-0.03561	3.2534	2	1	2	0	3	2	5004.5	1.17E-08
<b>Range independent:-</b>											
<b>Range : 5 km    Source depth : 92 m    Receiver depth : 92 m</b>											
1	-0.00851	0.008552	3.2727	19	20	0	0	39	0	5000.2	2.40E-07
2	-0.00464	-0.00463	3.2728	20	20	0	0	40	0	5000.2	1.54E-06
3	-0.00355	0.003573	3.2728	20	21	0	0	41	0	5000.2	2.68E-06
4	0.004652	0.004613	3.2728	20	20	0	0	40	0	5000.2	1.66E-06
5	0.005793	-0.0058	3.2728	20	19	0	0	39	0	5000.2	1.08E-06
<b>Range independent:-</b>											
<b>Range : 5 km    Source depth : 92 m    Receiver depth : 92 m</b>											
1	0.14678	-0.14118	3.2594	2	1	2	0	3	2	5009.8	4.59E-09

Range- distance between source to receiver,  $\theta_0$  - ray launching angle at source,  $\theta_r$  - ray angle at receiver,  $ds$  - ray path length,  $p_+$  - number of upper turning points,  $p_-$  - number of lower turning points,  $p_+ - p_-$  - number of top bonks,  $p_+ + p_-$  - number of bottom bonks,  $T$  - Travel time,  $I/I_0$  - acoustic intensity ratio.